JACS
JOURNAL OF THE AMERICAN CHEMICAL SOCIETY
Communication
pubs.acs.org/JACS

Enhanced Dipole Moments in Trimetallic Nitride Template Endohedral Metallofullerenes with the Pentalene Motif

Jianyuan Zhang,[†] Daniel W. Bearden,*[,‡] Tim Fuhrer,[†] Liaosa Xu,[†] Wujun Fu,[†] Tianming Zuo,[†] and Harry C. Dorn*[,†,§]

[†]Department of Chemistry, Virginia Polytechnic Institute and State University, Blacksburg, Virginia 24061, United States
[‡]National Institute of Standards and Technology, Chemical Sciences Division, Hollings Marine Laboratory, Charleston, South Carolina 29412, United States
[§]Virginia Tech Carilion Research Institute, Roanoke, Virginia 24016, United States

Supporting Information

ABSTRACT: Although not found to date in empty-cage fullerenes, the fused pentagon motifs (pentalenes) are allowed in endohedral metallofullerenes (EMFs). We have found that members of the trimetallic nitride template (TNT) EMF $Y_3N@C_{2n}$ (n = 39−44) family that contain pentalene motifs exhibit significant dipole moments. This finding is predicted to be significant for other EMFs with a metal atom orientated toward the pentalene motif. Chromatographic retention data and computational results for $Y_3N@C_2$-C_{78}, $Y_3N@C_s$-C_{82}, and $Y_3N@C_s$-C_{84} are examples that pentalene groups lead to a significant induced dipole moment (∼1D). A special case is the $Y_3N@C_2$-C_{78} that contains two pentalenes in a relatively small cage. The ^{13}C NMR spectrum for $Y_3N@C_2$-C_{78} exhibits strongly deshielded signals for the fullerene cage (155−170 ppm) supporting the presence of the pentalene motif. In addition, a lengthening of the covalent M−N bond in the internal M_3N cluster is found for all reported TNT EMFs that contain one or two pentalene motifs.

As advanced by Kroto, the isolated pentagon rule (IPR) states that there is a significant energy penalty for pentagons fused together on fullerene cages.[1] Although this seminal predictive tool was intended for "pristine" empty-cage fullerenes, the rule has been ostensibly extended to endohedral metallofullerenes (EMFs). The first EMFs with fused pentagons (pentalenes) were independently reported by Shinohara et al.[2] and Dorn et al.[3] for the molecules $Sc_2@C_{66}$ and $Sc_3N@C_{68}$, respectively, in 2000. Since then, the pentalene group has been found in almost all major families of EMFs, including monometallic EMFs,[4,5] dimetallic EMFs,[2,6,7] metal carbide fullerenes,[8] metal sulfide fullerenes,[9,10] and trimetallic nitride template (TNT) EMFs (metal nitride fullerenes),[3,11−19] which contribute most to pentalene-containing EMFs. To date, the structurally investigated TNT EMFs have adopted fullerene cages of D_3(6140)-C_{68},[3] C_{2v}(7854)-C_{70},[13] C_s(17490)-C_{76},[12] D_{3h}(5)-C_{78},[20] C_2(22010)-C_{78},[18] I_h(7)-C_{80},[21] D_{5h}(6)-C_{80},[22] C_s(39663)-C_{82},[16] C_s(51365)-C_{84},[11] D_3(19)-C_{86},[22] and D_2(35)-C_{88}.[22] On this list, the D_3-C_{68}, C_{2v}-C_{70}, C_s-C_{76}, C_2-C_{78}, C_s-C_{82}, and C_s-C_{84} isomers contain the pentalene groups.

Although there is a significant energy penalty for the antiaromatic 8 π-electron pentalene motif in empty-cage fullerenes, electron transfer from a metal to the pentalene nearby, creating a localized Hückel-aromatic system, can stabilize EMFs (Figure 1).[23] This reasoning is supported by multiple single-crystal X-ray studies where a metal ion is associated with a pentalene site with a localized negative charge.[9,11,15,16,18,24] Herein, we present evidence for significant dipole moments (∼1D) for those members of the $Y_3N@C_{2n}$ (n = 39−44) family with the pentalene motif. In addition, we predict significant dipole moments for other members of the $M_3N@C_{2n}$ family that contain an M−N bond oriented toward a pentalene motif. We also present the first ^{13}C NMR result for a member of the $M_3N@C_2$-C_{78} system that contains two pentalenes in a relatively small cage (C_{78}).

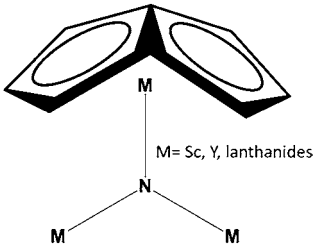

Figure 1. Fused pentagon motif and the trimetallic nitride cluster in pentalene-containing TNT EMFs.

The yttrium nitride cluster forms a family of TNT EMFs, $Y_3N@C_{2n}$ with n = 39−44,[17,25] which is a common range for many other metals, including Gd, Tb, and Tm. The C_2-C_{78} cage for $M_3N@C_{78}$ was initially proposed by Dunsch and co-workers.[14] Although limited sample quantities of $Tm_3N@C_{78}$ and $Dy_3N@C_{78}$ hampered their experimental structural study, their remarkable density functional theory (DFT) computations for $Y_3N@C_{78}$ predicted the C_2(22010)-C_{78} cage out of 24109 possibilities as the most stable cage for larger metal $M_3N@C_{78}$ systems. In 2009, the first unambiguous structural study of this family was reported by Balch and co-workers with the single-crystal structure of $Gd_3N@C_2$(22010)-C_{78}.[18] In this

Received: December 10, 2012
Published: January 24, 2013

   dx.doi.org/10.1021/ja312045t | J. Am. Chem. Soc. 2013, 135, 3351−3354

study, the striking differences between the UV−vis spectra for the $Gd_3N@C_2(22010)$-C_{78} and that for the $Sc_3N@D_{3h}(5)$-C_{78} was also reported to illustrate the importance of UV−vis data for establishing cage isomer features.[18] Wang and co-workers isolated $Y_3N@C_{78}$ and assigned it the $C_2(22010)$ cage based on spectral similarities to $Dy_3N@C_2$-C_{78} and $Gd_3N@C_2$-C_{78}.[19] In the current study, We have isolated a sample of $Y_3N@C_{78}$ from the ^{13}C-enriched EMF synthesis[26] performed by Luna Innovations, and its UV−vis absorptive features are in excellent agreement with the aforementioned studies of $M_3N@C_2(22010)$-C_{78}. The improved UV−vis peak resolution in Figure 2 compared to the previous $Y_3N@C_{78}$ report as well as

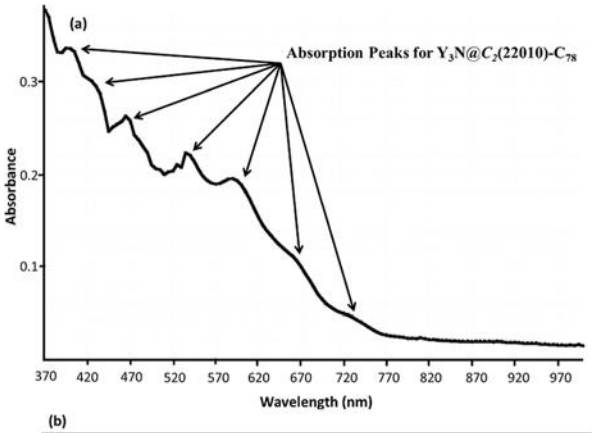

(b)

$M_3N@C_2$ (22010)-C_{78}	UV-vis absorption peaks (nm)
M=Dy[14]	410*, 460*, 560*, 600*, 670*, 730*
M=Gd[17]	410*, 460*, 550*, 590*, 670*, 730*
M=Y[18]	400†, 590†, 670†
M=Y (current study)	400, 420, 460, 540, 590, 670, 730

* These values are careful estimates obtained from corresponding references.[14,17]
† These values are reported by the authors in the corresponding reference.[18]

Figure 2. (a) UV−vis spectrum of the $Y_3N@C_2$-C_{78} with absorption peaks indicated. (b) Summary of absorption peaks for $M_3N@C_2(22010)$-C_{78} (M = Dy, Gd, Y).

similar absorption features for $Dy_3N@C_2$-C_{78} and $Gd_3N@C_2$-C_{78} confirm the same $C_2(22010)$-C_{78} cage for $Y_3N@C_{78}$ in the current study.[14,18,19]

The ^{13}C NMR spectrum for the ^{13}C-enriched $Y_3N@C_{78}$ is shown in Figure 3a. There are a total of 39 lines with

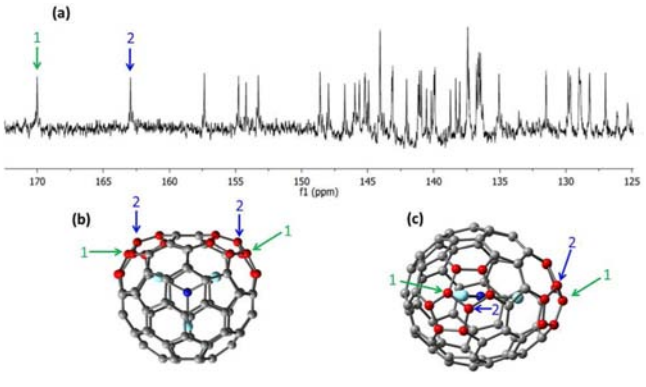

Figure 3. (a) 200 MHz ^{13}C NMR spectrum from an 800 MHz instrument of the $Y_3N@C_{78}$ in carbon disulfide/acetone-d_6 (v/v = 9/1) with 8 mg of $Cr(acac)_3$ as a relaxation agent; (b) top view; (c) side view optimized structure of $Y_3N@C_2$-C_{78} with the pentalenes highlighted.

approximately the same height suggesting a 39*2 pattern, with two highly deshielded peaks at 170.0 and 162.9 ppm, corresponding to the four carbon atoms on the [5,5,6] junction found only in pentalene-containing fullerene cages. In addition, there are 26 peaks corresponding to 52 carbon atoms on the [5,6,6] junctions and 11 peaks corresponding to 22 carbon atoms on the [6,6,6] junctions. The ^{13}C NMR spectrum is in agreement with the structural prediction for $Y_3N@C_{78}$[14] as well as the crystal study of $Gd_3N@C_{78}$,[18] suggesting the cage structure of $Y_3N@C_{78}$ is $C_2(22010)$-C_{78}. The smaller C_{78} cage is distorted by the two pentalene motifs that contribute to the deshielded signals from the four carbon atoms fusing the adjacent pentagons. Since the ^{13}C NMR chemical shift of carbon atoms on fullerene cages is related to several factors (including torsion strain[27]), deshielding of the ^{13}C NMR signals is in agreement with other ^{13}C NMR studies of pentalene-containing cages.[3,17] We note that the peak at 170.0 ppm is the most downfield ^{13}C NMR signal for a fullerene or metallofullerene cage observed to date, indicating a great amount of strain is associated with the two pentalene motifs on the oblate C_2 cage. This helps to localize the negative charge essential to the stabilization of the pentalene unit.

In addition, DFT computational structural optimization of $Y_3N@C_{78}$ has been independently performed based on the single-crystal structure of $Gd_3N@C_{78}$,[18] and the ^{13}C NMR chemical shift values were then calculated based on the optimized structure. The calculated values exhibit excellent agreement with the experimental results supporting the structural assignment of $Y_3N@C_2(22010)$-C_{78} (see Supporting Information). In both the view perpendicular (Figure 3b) and parallel (Figure 3c) to the TNT cluster, cage distortion near the pentalene sites (red) is clearly present.

The chromatographic retention behavior of the TNT EMF $Y_3N@C_{2n}$ family is compared with empty-cage fullerenes in Figure 4, utilizing a PYE (pyrenylethyl) column. Fuchs et al. showed that chromatographic data can be used to predict the dipole moments for EMFs.[28] Specifically, it is recognized that the retention mechanism between the solute (EMF) and chromatographic stationary phase (PYE, Figure 4a) consists of

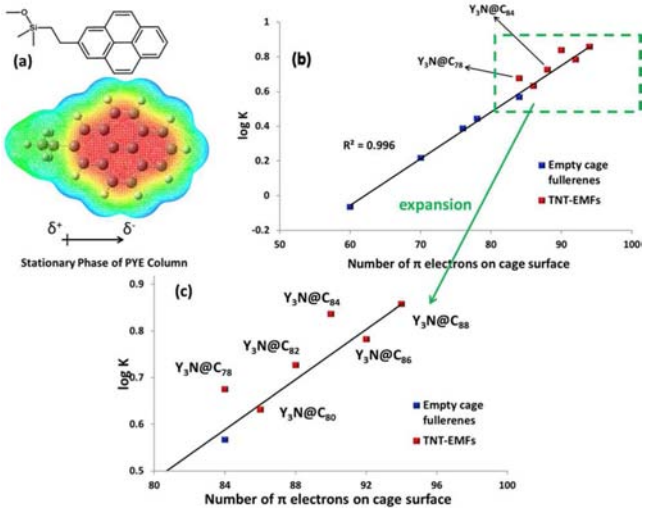

Figure 4. (a) The structure and electronic property of the stationary phase of PYE column. (b) Retention behavior of fullerenes (blue) and the $Y_3N@C_{2n}$ family (red) on PYE column. (c) Expansion of the framed area in (b) emphasizing the EMFs.

dx.doi.org/10.1021/ja312045t | J. Am. Chem. Soc. 2013, 135, 3351−3354

both $\pi-\pi$ interactions and dispersion forces, and the latter depends on the polarizability of the fullerenes (or EMFs) and the stationary phase. In addition, earlier studies have clearly demonstrated a linear relationship between the chromatographic capacity factor K ($K = (t_R - t_0)/t_0$, where t_R is the retention time and t_0 is the dead time) and the number of π electrons on empty fullerene cages,[28] as seen in Figure 4b (blue). For TNT EMFs (red), the number of π electrons equals the number of carbon atoms plus 6, due to the formal transfer of 6 electrons. In the cases of the IPR-allowed EMFs $Y_3N@I_h$-C_{80}, $Y_3N@D_3$-C_{86}, and $Y_3N@D_2$-C_{88}, the corresponding linearity (with the empty cages) is still maintained, even for widely different cage symmetries (Figure 4c). In contrast, the pentalene-containing $Y_3N@C_{2n}$ members $Y_3N@C_2$-C_{78}, $Y_3N@C_s$-C_{82}, and $Y_3N@C_s$-C_{84} all significantly deviate from the correlation with longer retention times, which suggests that those non-IPR members possess significant permanent dipole moments.

The DFT-calculated dipole moment values for the yttrium TNT EMF family (Figure 5) are consistent with the

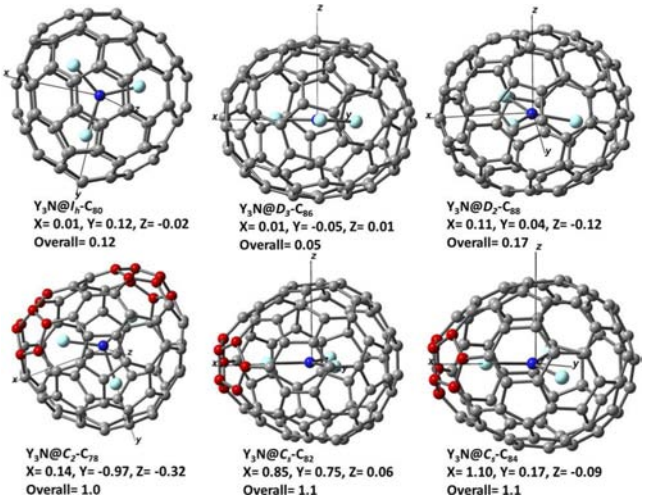

Figure 5. DFT-computed dipole moments of the $Y_3N@C_{2n}$ (n = 39–44) family (in Debye). The pentalene groups are highlighted in red.

chromatography retention time data. Namely, there is a clear gap between pentalene-containing species (overall dipole ≥1.0 D) and species without the pentalene motif (overall dipole <0.2 D). Specifically, the dipole moments of $Y_3N@C_2$-C_{78} and $Y_3N@C_s$-C_{84} are dominated by contributions from the cluster metal atom interaction with the pentalene group, leading to an induced dipole moment along that vector axis. The dipole moment for $Y_3N@C_s$-C_{82} is along two different vector axes, and the larger is along the pentalene-metal axis. As expected, there is no significant dipole moment for the TNT EMFs without pentalene groups, since there is no significant difference in the local 3-fold C_{3v} environment of the $(Y_3N)^{6+}$ cluster.

The prediction of a significant dipole moment for the pentalene-containing $Y_3N@C_{2n}$ EMFs also suggest lengthening of the covalent Y–N bond in the $(Y_3N)^{3+}$ cluster. In addition, M–N bond lengthening should be reflected in all TNT EMFs that have significant dipole moments, since the molecular dipole moment strongly depends on the charge time distance for the M–N bond vector (M and N have significantly different electronegativities). The lengthening of the M–N bond will break the symmetry of the M_3N cluster and lead to a nonzero dipole moment. As illustrated in Figure 6, available single-crystal data and DFT calculation results for all reported

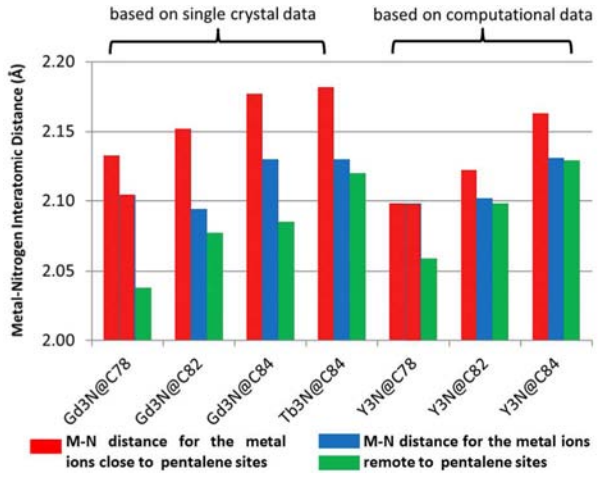

Figure 6. Metal–nitrogen distances in the $(M_3N)^{6+}$ cluster of pentalene-containing TNT EMFs.

members of the $M_3N@C_{2n}$ (M = Gd,[15,16,18] Tb,[11] and Y, n = 39–44) family that contain at least one pentalene motif show that they exhibit longer M–N bonds oriented toward the pentalene motif. The trend is even more convincing for the $Gd_3N@C_2$-C_{78} and $Y_3N@C_2$-C_{78} examples that contain two pentalene motifs for both experimental and DFT computational results. This bond lengthening could result from either a strong metal–pentalene interaction or the creation of extra space by the pentalene-caused cage distortion. In either mechanism, enhanced dipole moments for pentalene-containing TNT EMFs would be predicted.

In this paper, we predict significant dipole moments for lanthanide members of the $M_3N@C_{2n}$ (n = 39–44) family that contain an M–N bond oriented toward a pentalene motif. This prediction could also be extended to other pentalene-containing EMFs, but for the mono- and dimetallic EMFs, the case could be more complicated due to the noncentroid position of the endohedral ion(s).[28,29] The enhanced dipole moments will lead to improved solubility in polar solvents, and this could be an important consideration for utilizing EMFs in molecular optoelectronic devices and biomedical applications. For comparison, the dipole moment induced by the pentalene groups in TNT EMFs is comparable to that of azulene (1.08 D),[30] which has an ionic aromatic model and a solubility in water of 20 mg/L. Although the TNT EMF $Gd_3N@I_h$-C_{80} requires surface functionalization of the fullerene cage surface to impart water solubility for magnetic resonance imaging (MRI) contrast agent applications,[31] the enhanced dipole moment for $Gd_3N@C_2$-C_{78}, $Gd_3N@C_s$-C_{82}, and $Gd_3N@C_s$-C_{84} suggests the possibility that these EMFs could help alleviate this requirement, especially for lipid solubility applications. Finally, the finding of significant dipole moments for TNT EMFs containing the pentalene motif could also lead to the possibility of controlling molecular orientation in an external electric field.[29]

■ ASSOCIATED CONTENT

Ⓢ Supporting Information

Synthesis and characterization of $Y_3N@C_{78}$, computational methods, and correlation between experimental and computa-

dx.doi.org/10.1021/ja312045t | J. Am. Chem. Soc. 2013, 135, 3351–3354

tional chemical shift values. This material is available free of charge via the Internet at http://pubs.acs.org.

AUTHOR INFORMATION

Corresponding Author

dan.bearden@noaa.gov; hdorn@vt.edu

Notes

The authors declare no competing financial interests.

ACKNOWLEDGMENTS

We are grateful for the support of this work by the National Science Foundation [0938043] (H.C.D.). D.W.B. and H.C.D. acknowledge the support from the Hollings Marine Laboratory NMR Facility.

REFERENCES

(1) Kroto, H. W. *Nature* **1987**, *329*, 529.

(2) Wang, C. R.; Kai, T.; Tomiyama, T.; Yoshida, T.; Kobayashi, Y.; Nishibori, E.; Takata, M.; Sakata, M.; Shinohara, H. *Nature* **2000**, *408*, 426.

(3) Stevenson, S.; Fowler, P. W.; Heine, T.; Duchamp, J. C.; Rice, G.; Glass, T.; Harich, K.; Hajdu, E.; Bible, R.; Dorn, H. C. *Nature* **2000**, *408*, 427.

(4) Nikawa, H.; Kikuchi, T.; Wakahara, T.; Nakahodo, T.; Tsuchiya, T.; Rahman, G. M. A.; Akasaka, T.; Maeda, Y.; Yoza, K.; Horn, E.; Yamamoto, K.; Mizorogi, N.; Nagase, S. *J. Am. Chem. Soc.* **2005**, *127*, 9684.

(5) Wakahara, T.; Nikawa, H.; Kikuchi, T.; Nakahodo, T.; Rahman, G. M. A.; Tsuchiya, T.; Maeda, Y.; Akasaka, T.; Yoza, K.; Horn, E.; Yamamoto, K.; Mizorogi, N.; Slanina, Z.; Nagase, S. *J. Am. Chem. Soc.* **2006**, *128*, 14228.

(6) Kato, H.; Taninaka, A.; Sugai, T.; Shinohara, H. *J. Am. Chem. Soc.* **2003**, *125*, 7782.

(7) Yamada, M.; Wakahara, T.; Tsuchiya, T.; Maeda, Y.; Akasaka, T.; Mizorogi, N.; Nagase, S. *J. Phys. Chem. A* **2008**, *112*, 7627.

(8) Shi, Z. Q.; Wu, X.; Wang, C. R.; Lu, X.; Shinohara, H. *Angew. Chem., Int. Ed.* **2006**, *45*, 2107.

(9) Chen, N.; Beavers, C. M.; Mulet-Gas, M.; Rodriguez-Fortea, A.; Munoz, E. J.; Li, Y. Y.; Olmstead, M. M.; Balch, A. L.; Poblet, J. M.; Echegoyen, L. *J. Am. Chem. Soc.* **2012**, *134*, 7851.

(10) Chen, N.; Mulet-Gas, M.; Li, Y.-Y.; Stene, R. E.; Atherton, C. W.; Rodriguez-Fortea, A.; Poblet, J. M.; Echegoyen, L. *Chem. Sci.* **2013**, *4*, 180.

(11) Beavers, C. M.; Zuo, T.; Duchamp, J. C.; Harich, K.; Dorn, H. C.; Olmstead, M. M.; Balch, A. L. *J. Am. Chem. Soc.* **2006**, *128*, 11352.

(12) Yang, S.; Popov, A. A.; Dunsch, L. *J. Phys. Chem. B* **2007**, *111*, 13659.

(13) Yang, S.; Popov, A. A.; Dunsch, L. *Angew. Chem., Int. Ed.* **2007**, *46*, 1256.

(14) Popov, A. A.; Krause, M.; Yang, S.; Wong, J.; Dunsch, L. *J. Phys. Chem. B* **2007**, *111*, 3363.

(15) Zuo, T.; Walker, K.; Olmstead, M. M.; Melin, F.; Holloway, B. C.; Echegoyen, L.; Dorn, H. C.; Chaur, M. N.; Chancellor, C. J.; Beavers, C. M.; Balch, A. L.; Athans, A. J. *Chem. Commun.* **2008**, 1067.

(16) Mercado, B. Q.; Beavers, C. M.; Olmstead, M. M.; Chaur, M. N.; Walker, K.; Holloway, B. C.; Echegoyen, L.; Balch, A. L. *J. Am. Chem. Soc.* **2008**, *130*, 7854.

(17) Fu, W.; Xu, L.; Azurmendi, H.; Ge, J.; Fuhrer, T.; Zuo, T.; Reid, J.; Shu, C.; Harich, K.; Dorn, H. C. *J. Am. Chem. Soc.* **2009**, *131*, 11762.

(18) Beavers, C. M.; Chaur, M. N.; Olmstead, M. M.; Echegoyen, L.; Balch, A. L. *J. Am. Chem. Soc.* **2009**, *131*, 11519.

(19) Ma, Y.; Wang, T.; Wu, J.; Feng, Y.; Xu, W.; Jiang, L.; Zheng, J.; Shu, C.; Wang, C. *Nanoscale* **2011**, *3*, 4955.

(20) Olmstead, M. H.; de Bettencourt-Dias, A.; Duchamp, J. C.; Stevenson, S.; Marciu, D.; Dorn, H. C.; Balch, A. L. *Angew. Chem., Int. Ed.* **2001**, *40*, 1223.

(21) Stevenson, S.; Rice, G.; Glass, T.; Harich, K.; Cromer, F.; Jordan, M. R.; Craft, J.; Hadju, E.; Bible, R.; Olmstead, M. M.; Maitra, K.; Fisher, A. J.; Balch, A. L.; Dorn, H. C. *Nature* **1999**, *401*, 55.

(22) Zuo, T.; Beavers, C. M.; Duchamp, J. C.; Campbell, A.; Dorn, H. C.; Olmstead, M. M.; Balch, A. L. *J. Am. Chem. Soc.* **2007**, *129*, 2035.

(23) Slanina, Z.; Chen, Z.; Schleyer, P. v. R.; Uhlík, F.; Lu, X.; Nagase, S. *J. Phys. Chem. A* **2006**, *110*, 2231.

(24) Olmstead, M. M.; Lee, H. M.; Duchamp, J. C.; Stevenson, S.; Marciu, D.; Dorn, H. C.; Balch, A. L. *Angew. Chem., Int. Ed.* **2003**, *42*, 900.

(25) Fu, W.; Zhang, J.; Champion, H.; Fuhrer, T.; Azuremendi, H.; Zuo, T.; Zhang, J.; Harich, K.; Dorn, H. C. *Inorg. Chem.* **2011**, *50*, 4256.

(26) Zhang, J.; Fuhrer, T.; Fu, W.; Ge, J.; Bearden, D. W.; Dallas, J.; Duchamp, J.; Walker, K.; Champion, H.; Azurmendi, H.; Harich, K.; Dorn, H. C. *J. Am. Chem. Soc.* **2012**, *134*, 8487.

(27) Taylor, R.; Hare, J. P.; Abdulsada, A. K.; Kroto, H. W. *J. Chem. Soc., Chem. Commun.* **1990**, 1423.

(28) Fuchs, D.; Rietschel, H.; Michel, R. H.; Fischer, A.; Weis, P.; Kappes, M. M. *J. Phys. Chem.* **1996**, *100*, 725.

(29) Yasutake, Y.; Shi, Z. J.; Okazaki, T.; Shinohara, H.; Majima, Y. *Nano Lett.* **2005**, *5*, 1057.

(30) Anderson, A. G.; Steckler, B. M. *J. Am. Chem. Soc.* **1959**, *81*, 4941.

(31) Zhang, J.; Fatouros, P. P.; Shu, C.; Reid, J.; Owens, L. S.; Cai, T.; Gibson, H. W.; Long, G. L.; Corwin, F. D.; Chen, Z.-J.; Dorn, H. C. *Bioconjugate Chem.* **2010**, *21*, 610.